An Explanation for the Enhanced Activity for Light Alkane Conversion in Mildly Steam Dealuminated Mordenite: The Dominant Role of Adsorption

J. A. van Bokhoven,[*,1] M. Tromp,[*] D. C. Koningsberger,[*] J. T. Miller,[†] J. A. Z. Pieterse,[‡] J. A. Lercher,[‡] B. A. Williams,[§,2] and H. H. Kung[§]

[*]*Debye Institute, Department of Inorganic Chemistry and Catalysis, Utrecht University, Sorbonnelaan 16, 3508 TB Utrecht, The Netherlands;* [†]*BP Research Center, E-1F, 150 West Warrenville Road, Naperville, Illinois 60563;* [‡]*Faculty of Chemical Technology, University of Twente, 7500 AE Enschede, The Netherlands; and* [§]*Department of Chemical Engineering, Northwestern University, 2145 Sheridan Road, Evanston, Illinois 60208*

This paper presents a catalytic, spectroscopic, calorimetric study of mildly steam-dealuminated mordenite (H-MOR). With increasing steam partial pressures at 673 K there is increasing dealumination, the loss of Brønsted acid sites and the presence of extra-framework Al (Al_{EF}) likely in the zeolite pores. Additionally, the number of Lewis sites increases with increasing Al_{EF}. As observed in previous studies, the catalytic activity for hydroisomerization of *n*-hexane and monomolecular cracking of *n*-butane and *n*-hexane initially increases and goes through a maximum with increasing steam severity. While the maximum increase in the rate of hexane cracking is about 5 times, the activation energies indicate that steaming does not significantly change the strength of the Brønsted acid sites. In the absence of Al_{EF}, the enthalpy of alkane adsorption is constant at all surface coverages. However, in the presence of Al_{EF}, the initial heat of alkane sorption increases by about 5–10 kJ/mol. After covering these adsorption sites, the heat of adsorption is identical to that on the unsteamed H-MOR until saturation coverage has been reached. The increased enthalpies of adsorption are suggested to occur on the Al_{EF}, Lewis acid sites. Since the surface coverage of paraffins under typical reaction conditions is low, it is proposed that the enhanced rate is due to the increased initial heat of adsorption leading to a higher concentration of reactants in the steamed H-MOR zeolites. © 2001 Academic Press

Key Words: light alkane conversion; zeolite steaming; enhanced activity; adsorption; zeolite mordenite; cracking.

INTRODUCTION

Generally, it is assumed that the acidic properties of zeolites govern their activity, which explains why many studies have been devoted to the determination of the nature, the number, and the strength of acid sites (1, 2). Brønsted acidity is concluded to be very complex and affected by several factors such as the T–O–T angle (3, 4)

and the density of acid sites (5). It is well known that steaming reduces the concentration of Brønsted acid sites (6) creating extra-framework Al (Al_{EF}). These Al_{EF} species can remain within the micropores and may affect the catalytic activity. Several studies have correlated the presence of Al_{EF} species to the enhanced activity following mild steaming (7–15). It has been proposed that the Al_{EF} interact with the bridging oxide ion of the Brønsted acid site and withdraw electron density, which results in increased proton acidity and, thus, higher activity (7, 8, 14–17). Based on Cs poisoning studies, Haag *et al.* (18) concluded that about 4% of the total aluminum present in ZSM-5 has enhanced activity. Although enhanced activity is often proposed to be due to increased acid strength, there is little evidence for a change in the properties of the Brønsted sites by ^{1}H NMR (11) or infrared spectroscopy (10, 11). An alternate proposal (20, 21) suggests that Al_{EF} lead to the formation of Lewis acid sites, which are thought to increase the rate by increasing the rate of hydride abstraction (paraffins to olefins). For paraffin cracking, if hydride abstraction is the rate-determining step, increasing the rate of olefin formation leads to an enhanced cracking rate. Furthermore, the alkoxy species can also undergo hydride transfer to further enhance the rate through the bimolecular cracking pathway (22–24).

Several studies demonstrate that monomolecular cracking obeys Temkin's relation and is primarily governed by adsorption of the alkane (25–27). Longer alkanes display higher heats of adsorption and lower apparent activation energies. Likewise, smaller pore zeolites, which have higher enthalpies of adsorption, also have higher cracking activity. The higher rate is due to the increased concentration of reactants in the pores of the zeolite (28).

For hydroisomerization, identical conclusions have been drawn. Denayer *et al.* have shown that differences in hydroisomerization activity for alkanes of different chain length are governed by their physisorption properties (29).

---

[1] To whom correspondence should be addressed.

[2] Current address: BP Research Center, Naperville, IL 60563.

Likewise, van de Runstraat *et al.* have shown that the hydroisomerization activity of *n*-hexane over different zeolites may be explained by the different heats of sorption of *n*-hexane in the pores of these zeolites (30). Both studies conclude that the higher isomerization rates are due to the increased concentration of reactants within the pores, rather than due to differences in the strength of the acid sites.

While there is agreement that mild steam-dealumination of zeolites leads to higher catalytic activity, the reasons for these changes remain uncertain. The results of this catalytic, spectroscopic, calorimetric study of mildly steam-dealuminated mordenite indicate that the increased rate is not due to an increase in the Brønsted acid strength. The increased rate is suggested to be due to an increase in the initial heat of alkane adsorption on Lewis acid sites (Al_{EF}), which is thought to increase the concentration of reactants in the steamed zeolites under the reaction conditions.

EXPERIMENTAL

Catalysts

Na Mordenite (LZM-5) is commercially available from UOP and was ammonium exchanged and calcined prior to use (31). The H-mordenite contains 5.7% Al and 0.02% Na by elemental analysis, hence it is designated H-MOR57. A commercial H-mordenite, (CBV30A), was available from Zeolyst and contains 2.6% Al by elemental analysis and is called H-MOR26. H-MOR26 was subsequently steamed at 673 K for 3 h at different partial pressure of H_2O, Table 1, and the resulting samples are labeled S*XXX*, where *XXX* is the steam partial pressure. Sample S40024 was steamed at 673 K and 400 Torr H_2O for 24 h.

H-MOR catalysts (H-MOR57, H-MOR26, S400, and S40024) were impregnated with $Pt(NH_3)_4(OH)_2$ to give a Pt loading of 2.0 wt%. The Pt catalysts were dried overnight at 375 K and calcined in a 50 ml min^{-1} N_2/O_2 flow at 723 K

for 2 h at a rate of 0.5 K min^{-1}. The Pt dispersion, determined by volumetric hydrogen chemisorption, was between 30 and 40% for all samples.

The catalysts were characterized by XRF elemental analysis, N_2 BET surface area and pore-volume, X-ray powder diffraction, and ^{27}Al and ^{29}Si MAS NMR. The number of acid sites was determined by NH_3, *n*-propylamine and *i*-propylamine temperature programmed desorption (TPD). For the NH_3 TPD, the zeolites were NH_4^+ ion exchanged with NH_4NO_3, washed 3 times with water at room temperature, and dried at 375 K. Washing removes physisorbed but not chemisorbed NH_3, thus the number of acid sites is equivalent to the amount of desorbed NH_3, assuming 1 NH_3/H^+. For the latter of the two TPD methods, the number of acid sites was determined by the amount of amine decomposed to NH_3 and olefin at high temperature, which was determined by mass spectrometry (32). The number of Lewis and Brønsted acid sites was determined by IR spectroscopy of adsorbed pyridine. The band at 1456 cm^{-1} was used to quantify the amount of pyridine on accessible Al^{3+} cations, and the band at 1547 cm^{-1} was used to determine the quantity of Brønsted acid sites (pyridinium ions, PyH$^+$) (33). Physisorbed pyridine was observed near a band at 1446 cm^{-1} that disappeared completely after desorption in a stream of helium at 473 K. The extinction coefficients for the pyridine adsorbed on Lewis (1456 cm^{-1}) and Brønsted (1547 cm^{-1}) acid sites were 1.8 and 1.5, respectively (33).

Microcalorimetry and Gravimetry

The gravimetric and calorimetric measurements were performed in a modified SETARAM TG-DSC 111 instrument. The Mordenite samples were heated under vacuum at 10 K min^{-1} to 673 K and maintained at that temperature for one hour. After activation the sample was cooled to 323 K and dosed stepwise with the alkanes (C_3–C_6). Equilibration was assumed when no further changes in the heat flow and the uptake could be observed.

IR Spectroscopy

FTIR measurements were performed on a BRUKER IFS-88 spectrometer equipped with a flow cell and a vacuum cell. Approximately 3 mg of each *ex situ* precalcined sample was pressed into self-supporting wafers. The samples were activated in flowing helium at 673 K in order to remove moisture. A spectrum of the empty IR cell was used as reference (I_0) to convert the single beam spectra (I) into absorbance spectra ($\log I_0/I$). The latter were baseline-corrected in the region from 3800 to 1300 cm^{-1}. To correct for the varying sample thickness, the spectra were normalized by the integral intensity of the overtones of the lattice vibrational bands at 1972 and 1865 cm^{-1}. The IR spectra of adsorbed alkanes were determined at 323 K between 0.02 and 25 mbar.

TABLE 1

Sample Coding

Sample	Pretreatment	Steam[a] PpH$_2$O (Torr)	Time (hours)	Coding
LZM-5	none	—	—	H-MOR57
CBV30a	Chem. leached	—	—	H-MOR26
H-MOR26	Steamed	50	3	S50
H-MOR26	Steamed	100	3	S100
H-MOR26	Steamed	200	3	S200
H-MOR26	Steamed	300	3	S300
H-MOR26	Steamed	400	3	S400
H-MOR26	Steamed	700	3	S700
H-MOR26	Steamed	400	24	S40024

[a] At 675 K.

Kinetic Experiments

n-Butane cracking experiments were performed in a plug-flow, tubular quartz reactor. Catalysts were activated in flowing air by heating at 10 K min^{-1} to 823 K and holding at this temperature for 1 h. *n*-Butane cracking was carried out using 1% nC_4 in helium at 1 bar and 773 K. Approximately 100 mg of catalyst was diluted with quartz and passed over the catalyst at four different WHSV values, and a least square fit was used to calculate the first-order reaction constants. The conversion was varied between 1 and 5%. The activity of the catalysts was monitored as a function of time on stream between 10 and 60 min. The reactor effluent was analyzed by on-line gas chromatography with a flame ionization detector. Similar procedures were followed to determine first-order reaction constants for *n*-hexane cracking. The observed activation energies were determined as the slope of the linear, least square fit of the logarithm of the observed rate constant versus inverse temperature (28).

n-Hexane hydroisomerization was conducted in a plug-flow, tubular glass reactor, placed in a thermostatic oven. Mass flow controllers regulated the incoming H_2 flow. The *n*-hexane (Merck) was injected in the system using a high performance liquid chromatograph pump (Shimadzu LC-10AD). The reaction products were analyzed using a Perkin–Elmer AutoSystem XL Gas Chromatograph with a Chrompack capillary column CP Sil 5 CB 0.53 mm 50 m. The whole system was heated to avoid condensation of gases.

Prior to catalytic testing the samples were reduced at 623 K (at a rate of 5 K min^{-1}) for one hour and subsequently cooled in H_2 to the reaction temperature, ranging from 423 to 623 K. Approximately 100 mg of catalyst, with a particle size of 150–500 μm, an *n*-hexane flow of 0.118 mmol min^{-1}, and an H_2 flow of 25 ml min^{-1} at a total pressure of 1 bar were used. Conversions were kept below 5% by varying the amount of catalyst and *n*-hexane/H_2 flow at a constant $H_2 : C_6$ mole ratio of 9.

RESULTS

The surface area and pore volumes of the zeolites are given in Table 2. Although the micropore volume of H-MOR57 and H-MOR26 were identical within experimental error, the BET, external surface area, and mesopore volume of H-MOR26 were significantly larger than that of H-MOR57. The increased mesopore volume and lower Al content of H-MOR26 suggest that it has been dealuminated by strong acid (34). The surface area, micropore, and mesopore volumes of the steam-dealuminated mordenites were similar to those of the starting zeolite.

The ^{27}Al NMR spectrum of H-MOR26 indicated that 15–20% of the Al was not in the framework, Table 3. This Al_{EF} was present in an octahedral coordination (0 ppm resonance) (35). Steaming with increasing partial pressure of H_2O, or for longer time, led to further dealumination. The

TABLE 2

Nitrogen Physisorption Results

Sample	BET (m^2/g)	Micropore Volume (cm^3/g)	Mesopore Volume[a] (cm^3/g)	EXT. area (m^2/g)[b]
H-MOR57	525	0.19	0.04	24
H-MOR26	584	0.20	0.11	90
S50	573	0.19	0.11	98
S100	604	0.21	0.10	93
S200	594	0.21	0.09	73
S300	593	0.20	0.12	89
S400	602	0.21	0.11	92
S700	588	0.20	0.11	99
S40024	588	0.18	0.15	119

[a] Pores with diameter 2 < D < 50 nm.
[b] Surface area of pores larger than 2 nm.

amount of octahedral Al remained approximately constant, while a broad resonance between about 40 and 20 ppm increased with increasing dealumination. The fraction of Td Al, i.e., structural Al with a resonance at 55 ppm (35), removed by steaming ranges from about 0.05 (50 Torr) to 0.45 (400 Torr for 24 h).

The ^{29}Si NMR spectra confirmed the loss of framework Al; however, the changes in the Si/Al ratio were small until there was significant loss of framework Al (Table 4). The XRF elemental analysis of H-MOR26 and steamed mordenites indicate that no Al was lost from the sample upon steaming.

The number of acid sites was determined by temperature-programmed desorption of ammonia and *n*-propylamine and *i*-propylamine decomposition (Table 4). There was good agreement between the amount of adsorbed ammonia and structural Al determined by the combination of the elemental analysis and ^{27}Al NMR. For example, in H-MOR26, the elemental analysis was 2.6% Al and the ^{27}Al NMR indicated that 82.5% was Td Al, or 0.79 mmols of structural Al. The amount of adsorbed NH_3 was 0.74 mmol. With increasing steam partial pressure (or time) the amount of adsorbed NH_3 decreased indicating a decrease in the number of acid sites. Although the amounts of adsorbed *n*-propyl and *i*-propylamine were slightly higher than that for NH_3, the trends with steaming were similar. Since the number of acid sites decreased with increasing steam severity, but the

TABLE 3

Relative Intensity of Aluminum Species Determined by ^{27}Al MAS NMR

Sample	H-MOR26	S50	S100	S200	S400	S700	S40024
Td	77	78	66	60	61	50	45
"30 ppm"	0	0	11	17	19	28	34
Oh	23	22	23	23	20	22	21

TABLE 4

Physico-chemical Characterization of the Mordenite Samples

Sample	Si/Al[a]	Si/Al[b]	nPA[d] mmol/g	iPA[e] mmol/g	Al/u.c.[b]	FAl[b] mmol/g	NH$_3$[c] mmol/g	ratio[f] BA/LA	u.c.[h] (Å^3)
H-MOR57	6.0	5.74	2.21	1.47	7.12	2.11	2.25	124[g]	2769
H-MOR26	20.2	15.5	1.12	1.10	2.90	0.96	0.74	11	2730
S50	20.3	n.d.[i]	n.d.	1.00	n.d.	0.87	0.72	8	2723
S100	20.2	13.2	n.d.	0.85	3.37	1.00	0.71	5.5	2729
S200	20.3	13.7	n.d.	1.05	3.24	1.04	0.71	5.5	2731
S300	20.2	13.3	n.d.	0.78	3.35	0.99	0.64	5.2	n.d.
S400	20.2	15.6	0.80	0.79	2.90	0.85	0.58	4.4	2732
S700	20.2	35.2	n.d.	0.65	1.32	0.33	0.48	2.8	2737
S40024	20.3	52.5	0.50	0.51	0.90	0.27	0.34	1.5	2735

[a] XRF.

[b] ^{29}Si MAS NMR.

[c] NH$_3$ adsorption.

[d] n-propylamine TPD.

[e] i-propylamine TPD.

[f] Pyridine ad/desorption, BA = Brønsted Acid site; LA = Lewis Acid site.

[g] 40% of total sites is covered.

[h] X-ray diffration, u.c. = unit cell.

[i] n.d. = not determined.

total content of Al remained constant, the Al$_{EF}$ species do not adsorb these bases quantitatively and, thus, were not strongly acidic.

For H-MOR57, the amount of adsorbed NH$_3$ (2.25 mmol) was again similar to the elemental analysis, 5.7% Al and 100% Td or 2.19 mmol Al. While the amount of adsorbed n-propylamine was similar to that of NH$_3$, the amount of i-propylamine was significantly lower suggesting a steric limitation for the more bulky base.

The IR spectrum of adsorbed pyridine (33) indicated that H-MOR57 had few Lewis acid sites (Table 4), although only about 40% of the Brønsted sites adsorbed pyridine. As observed with i-propylamine, not all acid sites in H-MOR57 were accessible to large bases. In the (unsteamed) H-MOR26, there was a small number of Lewis sites. The ratio of Brønsted/Lewis sites decreased sharply with increasing steam partial pressure due to both an increase in the number of Lewis sites and a decrease in the number of Brønsted sites.

X-ray diffraction data showed a significant decrease in unit cell volume of H-MOR26 compared to H-MOR57, which was consistent with the lower Al content of the former (36). However, after steaming there was a small gradual increase in unit cell volume. While temperature-programmed desorption by NH$_3$, n-propylamine, i-propylamine, ^{27}Al and ^{29}Si NMR all indicated increasing dealumination, there was not a corresponding decrease in the XRD unit cell size that would be expected. Although the XRD unit cell size generally decreases with decreasing amounts of framework Al, ion exchange of ammonium, calcium, or rare earth ions leads to an expansion of the unit cell in Y zeolite (37). It is possible, therefore, that the small expansion of the unit cell size with decreasing framework Al was due to the presence of Al$_{EF}$ species or aluminum ions within the steamed MOR pores. However, varying conditions during the XRD-measurements, such as the water content, will also effect the XRD results.

The initial characterizations of the catalysts indicated that H-MOR57 was highly crystalline with few mesopores. There was a large number of Brønsted acid sites with few Lewis sites, although not all Brønsted sites were accessible to bulky bases. H-MOR26 was also highly crystalline, however, there was a significant number of mesopores. In H-MOR26, there were fewer Brønsted sites (due to the lower Al content) along with a small number of Lewis sites. Increasing steam partial pressures at 673 K led to increasing dealumination, the loss of Brønsted acid sites and the presence of Al$_{EF}$ in the zeolite pores. Additionally, the number of Lewis sites increased with increasing Al$_{EF}$.

Alkane Cracking and Isomerization

The rate constants per Brønsted acid site (determined by NH$_3$ TPD) of n-butane and n-hexane conversion were determined at 773 K from the slope of the conversion–WHSV plots fitting first-order kinetics. The catalysts were stable with time on stream. Selectivities were identical to those previously reported (25, 38) showing that the monomolecular pathway was the dominant reaction. The turnover frequency (TOF) for n-butane cracking over H-MOR26 was 0.62 10^{-4} molecules/s · H$^+$. In Fig. 1, it is shown that the n-butane cracking activity initially increased with mild steaming, went through a maximum at higher H$_2$O partial pressures, and finally decreased at the highest level of
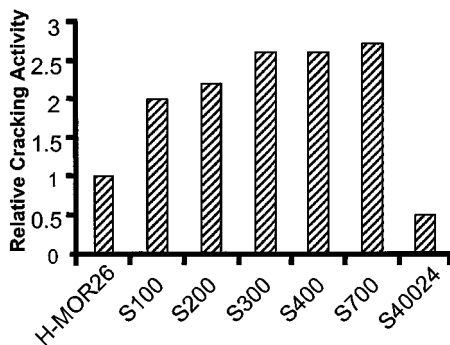
FIG. 1. Relative n-butane monomolecular cracking activities at 773 K and 1 bar (1% n-butane in He). The turnover-frequency (TOF) for n-butane cracking over H-MOR26 was 0.62 10^{-4} molecules/sec · H$^+$.

TABLE 5

Rate Constant for n-Hexane Hydroisomerization at 523 K and 1 bar Total Pressure

Catalyst	Rate constant {mmol/(mol sites. s.kPa)}
H-MOR57	0.41[a]
H-MOR26	6.3
S400	50
S40024	11

[a] Estimated number of sites in 12 MR from i-propyl amine decomposition.

dealumination (all rate constants are normalized to that of H-MOR26). At steam partial pressures from about 300–700 Torr the maximum activity per H$^+$ site was 2.5 times higher than that of (unsteamed) H-MOR26. The activity per gram of these catalysts was also about two times that of H-MOR26. H-MOR26 steamed at 400 Torr for 24 h was about half as active as unsteamed catalyst.

For monomolecular n-hexane cracking, the observed rate constant based on the number of Brønsted sites for H-MOR26 was 1.5 [(mmol)(mol sites)$^{-1}$(s)$^{-1}$(kPa)$^{-1}$] at 773 K. As observed for n-butane cracking, the n-hexane cracking rate constant of S400 was higher than that of (unsteamed) H-MOR26, 7.4 [(mmol)(mol sites)$^{-1}$(s)$^{-1}$(kPa)$^{-1}$], an increase of 4.9 times. The rate constants were determined at 753, 773, 793, and 813 K. The apparent activation energies were determined from the Arrhenius expression and were identical within experimental error, 157 $\pm$ 9 and 153 $\pm$ 9 kJ/mol for the H-MOR26 and S400, respectively. In contrast, the preexponential factors, increased from 4.0 $\times$ 10^{14} (s)$^{-1}$(kPa)$^{-1}$ for the H-MOR26 to 1.1 $\times$ 10^{15} (s)$^{-1}$(kPa)$^{-1}$ for the higher activity S400 (Fig. 2). In contrast with the n-butane experiments, selectivities to ethene, propene, and particularly butene isomers varied considerably with conversion. How-
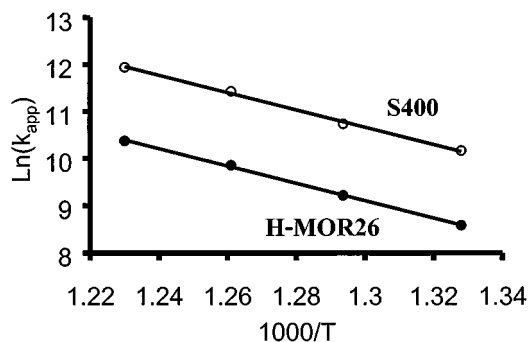
ever, this is mainly the result of secondary cracking reactions of the larger alkene products, such as hexene, to form smaller alkenes (27). Molar selectivities to hydrogen and methane, which can only be products of monomolecular reactions, remained constant over the range of conditions studied.

The activity of 2-wt% Pt loaded H-MOR57, H-MOR26, S400, and S40024 for hydroisomerization of n-hexane was studied at 523 K by varying the WHSV to obtain 1% conversion. The rate constants per Brønsted site (determined by NH$_3$ adsorption) are shown in Table 5. Although H-MOR57 had the highest number of Brønsted acid sites, its activity was the lowest of all the catalysts. It is likely that this results from diffusion limitations in the one-dimensional mordenite pores (31). The crystals of H-MOR57 are well formed and n-hexane must diffuse the length of the pore to access all acid sites. By contrast, the mesopores in H-MOR26 shorten the diffusion path; thus, although there were fewer Brønsted sites, the activity was higher. Diffusion measurements under catalytic conditions were performed in a tapered element oscillating microbalance (TEOM) in our laboratory (39). These measurements identified a diffusion-controlled reaction in the parent, untreated mordenite that was largely alleviated after mesopore creation in the crystallites. The selectivity of the two catalysts was also consistent with differences in diffusivity. In H-MOR57, the selectivity to di-methyl isomers and cracked products was significantly higher than that in H-MOR26, while the selectivity to mono-methyl isomers was higher in the latter (31). As observed for n-butane and n-hexane cracking, S400 was about eight times more active than H-MOR26. While S40024 was again less active than S400, the former was about twice as active as the (unsteamed) H-MOR26. The selectivities on these more active samples, S400 and S40024, display a shift toward isomerization. These samples showed selectivity to monobranched and dibranched isomers of 96.5 and 98%, respectively (40).

IR Spectroscopy with and without Adsorbed Alkane

Figure 3 shows the IR spectra of H-MOR57, H-MOR26, S100, S400, and S40024. The IR spectrum of H-MOR57
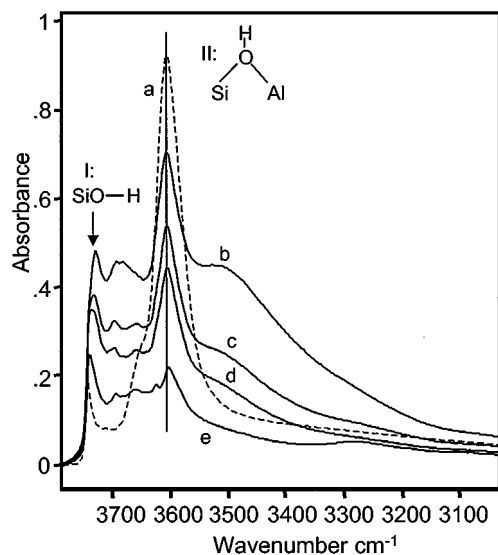

FIG. 2. Temperature dependence of the apparent rate constant of n-hexane monomolecular cracking on H-MOR26 (bottom line) and S400 (top line).

FIG. 3. Infrared spectra taken at 373 K. a.) H-MOR57 (dashed line), b.) H-MOR26, c.) S100, d.) S400 and e.) S40024.
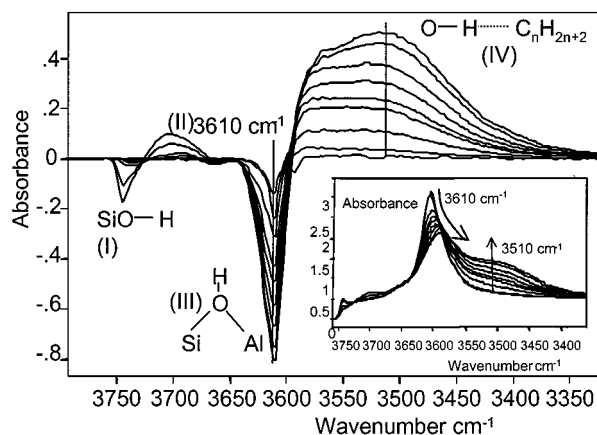

FIG. 4. Difference infrared spectra of the OH bands in H-MOR57 with increasing partial pressure of n-butane. Consecutive lines indicate an increasing loss (negative) or gain (positive) in intensity of the IR bands with increasing butane pressure. The inset shows the absorbance spectra and the shift of Si-OH-Al band with increasing n-butane surface coverage.

(Fig. 3a, dashed line) exhibited bands at 3744 and 3607 cm^{-1} assigned to OH stretching vibrations of terminal silanol (I: SiOH) and Brønsted acid sites (II: bridging Si–OH–Al) groups, respectively. For H-MOR26 (Fig. 3b), the intensity of the 3607 cm^{-1} band was significantly lower while the intensity of the silanol band was higher and broadened with the maximum shifted to a slightly lower wavenumber, 3730 cm^{-1}. This suggests the presence of lattice defects (41). There was a broad absorption from 3700 and 3400 cm^{-1}, which may be due to hydrogen-bonded silanol nests (42) or to the presence of water. Steaming at 100 Torr (Fig. 1c) further reduced the intensity of the Brønsted hydroxyl band. In addition, the broad hydrogen-bonded silanol band decreased. There were several bands between 3600 and 3700 cm^{-1}, which were similar to those from alumina (43). With increasing steam severity (see Figs. 3d and 3e) there was a further reduction in the intensity of the Brønsted hydroxyl band consistent with a decrease in the number of acid sites measured by TPD.

The acidic hydroxyl band at 3607 cm^{-1} in mordenite has been frequently reported to have two contributions, 3612 and 3585 cm^{-1}, assigned to OH groups in the main channels and side pockets, respectively (44). For our samples, the maximum of the 3607 cm^{-1} band did not shift by any significant extent indicating the simultaneous dealumination from the main channels and the side pockets.

The interaction of the mordenite hydroxyl groups with n-butane (at pressures between 0.02 and 25 mbar) can be observed for H-MOR57, H-MOR26, and S400 in Figs. 4, 5, and 6, respectively. On H-MOR57, both the silanol (3744 cm^{-1}, peak I) and Brønsted acid bands (3607 cm^{-1}, peak II) decreased with increasing n-butane partial pressure (see inset in Fig. 4). In parallel, a broad band appeared

at lower wavenumber indicating hydrogen-bonding interaction for both the silanol (peak III) and the bridging acid site (peak IV). The intensity of the acidic hydroxyl band decreased to 75% of its original value and did not change further at higher pressures, suggesting that at saturation coverage only 25% of the Brønsted acid sites interact with n-butane. The partial reduction in the intensity of the acidic band suggests that these Brønsted sites were predominantly in the large channel.

For H-MOR26 (Fig. 5), the intensity of the Brønsted hydroxyl groups decreased with increasing n-butane partial pressure. However, in contrast to H-MOR57, at high partial pressures, the intensity of the Brønsted peak disappeared indicating that all acid sites are accessible to n-butane. Consistent with the smaller number of Brønsted
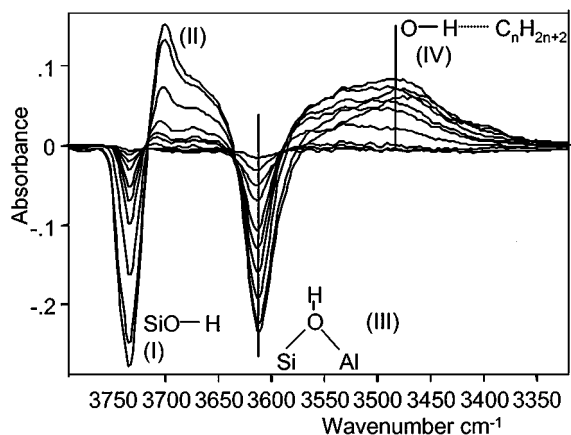

FIG. 5. Difference infrared spectra of the OH bands in H-MOR26 with increasing partial pressure of n-butane. Consecutive lines indicate an increasing loss (negative) or gain (positive) in intensity of the IR bands with increasing butane pressure.
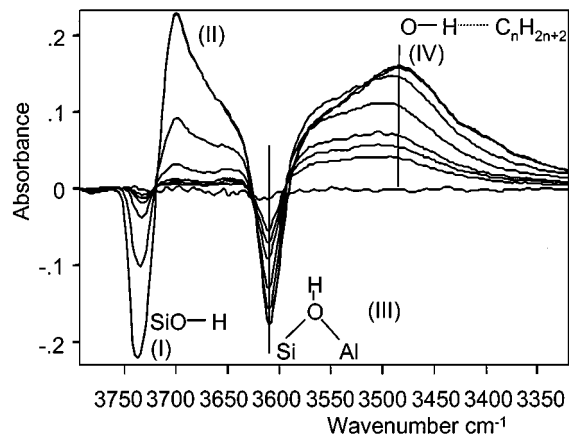
FIG. 6. Difference infrared spectra of the OH bands in S400 with increasing partial pressure of n-butane. Consecutive lines indicate an increasing loss (negative) or gain (positive) in intensity of the IR bands with increasing butane pressure.

FIG. 8. The surface coverage dependent enthalpy of alkane adsorption for H-MOR57 at 323 K.

sites, the intensity of the broad adsorption due to hydrogen bonded n-butane (from 3600 to 3350 cm^{-1}) was smaller than that in H-MOR57. Although the loss in the intensity of the silanol band was roughly equivalent to that in H-MOR57, there was a significant increase in the intensity in the broad band between 3600 and 3740 cm^{-1}. Furthermore, this band was significantly broader and had a different shape than that in H-MOR57. The intensity of this latter band further increased with steaming, Fig. 6.

Sorption of Light Alkanes

Figure 7 shows the averaged heat of adsorption for propane, n-butane, n-pentane, and n-hexane on H-MOR57, H-MOR26, S400, and S40024, before saturation coverage was reached (and excluding an increased heat of sorption at the lowest coverages, *vide infra*). The enthalpy of sorption
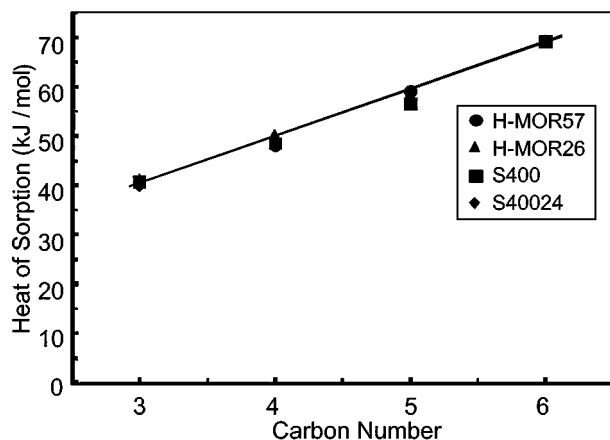
increased linearly with the chain length by about 10 kJ/mol per additional CH$_2$ and was identical for all the samples. Although the average heat of sorption did not vary among the samples, there were differences as a function of coverage. For H-MOR57, the heat of alkane sorption remained constant at all surface coverages then decreased at saturation coverage visible for pentane (see Fig. 8). For H-MOR26, shown in Fig. 9, the enthalpy of alkane adsorption at low surface coverage was about 5 kJ/mol higher than that at higher coverage. Approximately 10% of the alkane was more strongly adsorbed. S400 showed similar sorption characteristics, (see Fig. 10); however, the initial heat of adsorption was higher by about 10 kJ/mol and about 20% of the alkane were more strongly adsorbed. A comparison of the enthalpies of adsorption for the different catalysts versus surface coverage for propane is shown in Fig. 11. The heats of sorption at higher coverage (excluding the initial coverage) are identical for all samples. However, different heats

FIG. 7. The average enthalpy of adsorption of propane, n-butane, n-pentane and n-hexane for H-MOR57, H-MOR26, S400 and S40024, taken at coverages below saturation coverage (and excluding the initial increase in heat of sorption).
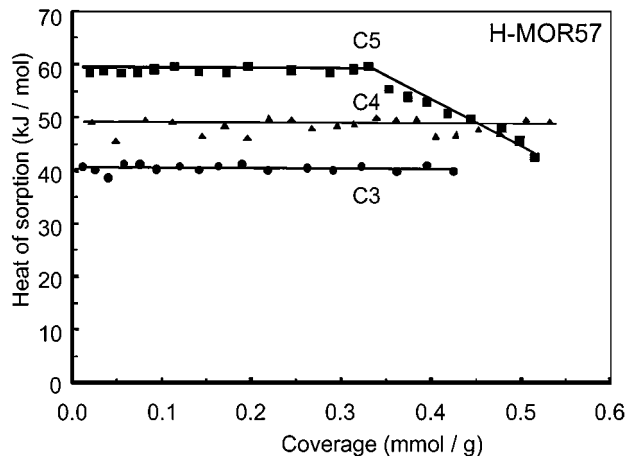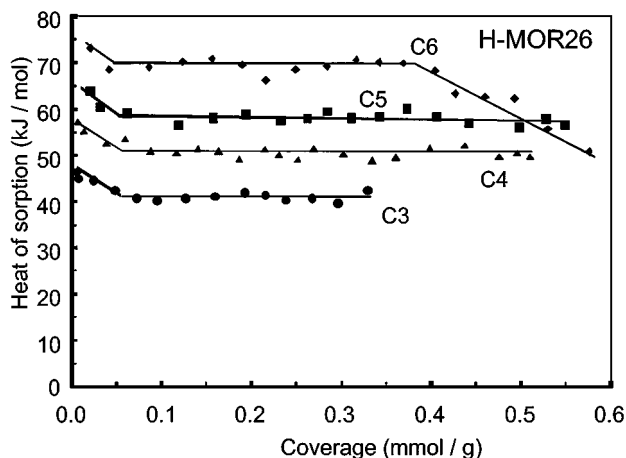

FIG. 9. The surface coverage dependent enthalpy of alkane adsorption for H-MOR26 at 323 K.
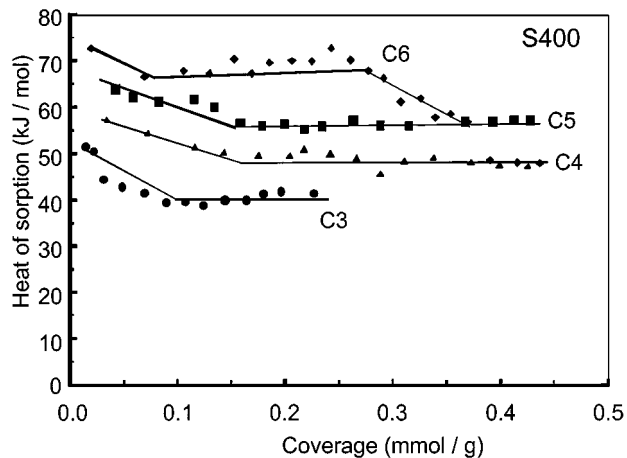
FIG. 10. The surface coverage dependent enthalpy of alkane adsorption for S400 at 323 K.

of sorption between the samples are clear at the initial coverages. Steaming increases the heat of sorption at the initial coverages. S400 shows the highest heat of sorption.

DISCUSSION

At high temperature and low alkane partial pressures, cracking of alkanes proceeds predominantly by the monomolecular cracking pathway (45, 46). The high selectivity to H_2, CH_4, and C_2H_6 in this study strongly suggests that the monomolecular pathway dominates for n-butane and n-hexane cracking. Since the rate-determining step involves the protonation of the alkane, the rate of reaction is dependent on the number and intrinsic strength of the Brønsted acid sites and the surface concentration of alkane.

In contrast, hydroisomerization is a bifunctional reaction. The alkane is rapidly dehydrogenated on Pt to an equilibrium composition of olefin-paraffin. Due to its high
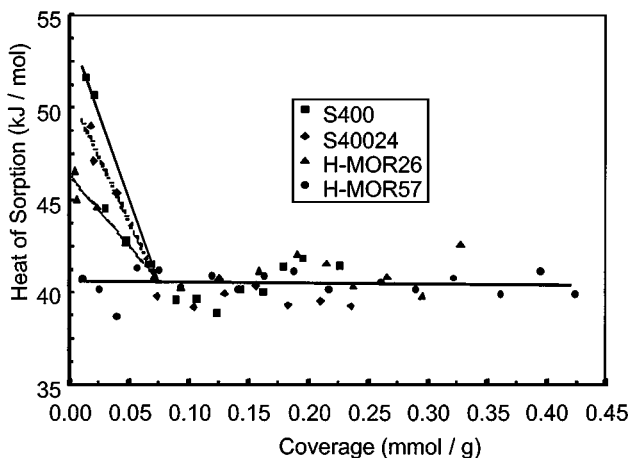

FIG. 11. The surface coverage dependent enthalpy of propane adsorption for H-MOR57, H-MOR26, S400 and S40024 at 323 K.

reactivity, the olefin is readily protonated, and the rate-determining step is skeletal-isomerization of the alkoxy species (47). The rate of the reaction is again dependent on the number and strength of the Brønsted acid sites and the surface concentration of olefin. Since the olefin is in equilibrium with paraffin, however, the surface coverage will parallel one another.

For both alkane cracking and hexane hydroisomerization, mild steaming leads to increased activity; however, severe steaming causes a decrease in activity. For alkane cracking, the maximum increase in activity was about 3 to 5 times that of (unsteamed) H-MOR26. The maximum increase in activity for hydroisomerization was slightly larger, about eight times that of H-MOR26. For all reactions, the maximum in activity was obtained for the S400 catalyst. In the latter, there were approximately 20% fewer Brønsted sites than in H-MOR26. For n-butane and n-hexane cracking, further steaming (S40024) leads to increased dealumination and lower activity, about half that of H-MOR26. In contrast, the hydroisomerization activity of S40024 is still twice that of H-MOR26. These results are consistent with previous studies on the effect of mild steam dealumination in other zeolites (18, and references therein).

Several explanations have been proposed to account for the enhanced activity due to mild steam dealumination. For example, Al_{EF} species are suggested to interact with nearby Brønsted acid sites creating sites with increased acid strength (7, 14–18). The Al_{EF} is thought to coordinate to the Si–O–Al bridging hydroxyl group reducing the oxygen electron density producing enhanced Brønsted acidity. Since two Al ions are required for a single active site (one lattice and one Al_{EF}) the increase in activity should correlate with the number of next nearest neighbor Al ions in the unsteamed zeolite as has been observed (7, 8, 14, 16, 17). Haag estimated that ca. 1 to 5% of the Brønsted sites in ZSM-5 have enhanced activity (18). If 1 to 5% of the sites do have enhanced activity, an activity increase by a factor of 3 to 5 means that "super acidic" sites are 40 to 500 times more active than a "normal" Brønsted acid site. While such a small number of super active sites might not be easily detected spectroscopically, these sites should have a significantly lower activation energy. The apparent activation energies for n-hexane cracking for H-MOR26 and S400 are 157 and 153 ± 9 kJ/mol, respectively. These activation energies are very similar. This is not in agreement with the presence of only a few sites with high activity. Thus it is concluded, that the increase in activity cannot be explained by the presence of a small number of super-active, Brønsted acid sites. Similar conclusions have recently been made for mildly steamed and sodium poisoned ZSM-5 and Y zeolites (11, 48).

An alternate proposal suggests that Lewis acid sites participate in the catalytic process and have higher activity

for hydride transfer than Brønsted sites (20, 22–24, 49). This bifunctional mechanism, where Lewis sites generate olefins that react on Brønsted sites, implies that there is a balance in the number of each site for maximum activity and that the activity should initially increase and go through a maximum with increasing dealumination. While such a proposal could explain the results for alkane cracking, this mechanism is not consistent with the results in this study for hexane hydroisomerization. For isomerization, olefin formation via hydride abstraction is not rate limiting since olefins are rapidly formed on the metal. Furthermore, any enhancement in the rate of olefin formation would have no influence on the isomerization rate since olefins are in equilibrium with the alkane. Moreover, no clear relationship exists between the activity and the number of Lewis acid sites. Samples S300 and S400 show similar (enhanced) activity, but have large differences in the number of Lewis acid sites, while the number of Brønsted acid sites decreases slightly, see Table 4. Therefore, it is concluded that Lewis sites do not participate in the catalytic process and that the abstraction of hydride ion from paraffins is not the reason for the enhanced activity (50).

We suggest an alternate explanation for the increased activity of mildly steamed zeolites. For a first-order, heterogeneous reaction like monomolecular cracking or hydroisomerization of alkanes, the Langmuir–Henshelwood expression is

$$d(P_{HC})/dt = -k_{int} * K_{ads} * P_{HC}/[1 + K_{ads} * P_{HC}], \quad [1]$$

where k_{int} is the intrinsic rate constant, K_{ads} is the equilibrium adsorption constant of the reactant, and P_{HC} is the hydrocarbon partial pressure. K_{ads} has the effect of increasing the concentration of alkane in the pores relative to that in the gas phase. At high temperature and low alkane concentration, the expression simplifies (where $K_{ads} * P_{HC} \ll 1$) to

$$d(P_{HC})/dt = -k_{int} * K_{ads} * P_{HC}. \quad [2]$$

In Fig. 2 the apparent rate constant, (k_{app}) is given, which is the product of the intrinsic rate constant times the equilibrium adsorption constant

$$k_{app} = k_{int} * K_{ads}. \quad [3]$$

An increase in the rate, as observed for mildly steamed zeolite, is often interpreted as due to an increase in the intrinsic rate constant. This increase is then explained in terms of an increase in the Brønsted acid strength. However, it is also possible that the increase is due to an increase in the equilibrium adsorption constant, K_{ads}. The effect of an increase in K_{ads} is to increase the surface concentration of adsorbed alkane. Thus, the rate can also increase without a change in the strength of the acid site.

The temperature dependence of the apparent rate constant is given by (via $-RT \ln(K_{ads}) = \Delta G_{ads}$)

$$k_{app} = A_o * e^{-Eapp/RT} = A_o * e^{-Eint/RT} * e^{-\Delta Gads/RT} \quad [4]$$

$$= A_o * e^{-Eint/RT} * e^{-\Delta Hads/RT} * e^{\Delta Sads/R}. \quad [5]$$

Assuming that ΔS_{ads} is approximately constant, one obtains the Temkin equation:

$$E_{app} = E_{int} + \Delta H_{ads}. \quad [6]$$

The apparent activation energy is lower than the intrinsic activation energy by an amount equal to the enthalpy of adsorption. In order to evaluate changes in the intrinsic activation energy, one must also determine the contribution from the heat of adsorption.

Three examples demonstrate the importance of the sorption thermodynamics on the rate of the reaction. The rate for n-alkane cracking increases with increasing chain length with a corresponding decrease in the apparent activation energy that is compensated for by the increased heat of adsorption. The intrinsic activation energy, therefore, is independent of the carbon chain length (26, 27, 51). The higher reactivity of larger hydrocarbons is due to their higher concentration in the molecular sieve pores and not to their intrinsically higher reactivity. Similar results were obtained by Lercher *et al.*, who after correcting for the heat of sorption, found identical intrinsic activation energies for monomolecular cracking of different n-alkanes over H-ZSM-5 (25).

Likewise, the n-hexane cracking rate is dependent on the structure of the zeolite with H-ZSM-5 > H-MOR > H-USY. Again the differences are often suggested to be due to the higher acid strength of Brønsted sites in ZSM-5 compared to H-USY, for example. Determination of the apparent activation energies, however, indicates that the differences in activity are accounted for primarily by the differences in heat of sorption of the alkane. The conclusion is that the increased rate of reaction in zeolites of different structure is due to the increased heat of adsorption and higher concentration of reactants in the smaller pore zeolites, rather than due to a change in the acid strength (28, 48).

Finally, the rate of hydroisomerization is dependent on the size of the alkane (29) and the structure of the zeolite (30). Again, by evaluation of changes in the observed activation energy, the differences in rate may be accounted for by changes in the heat of adsorption, rather than by changes in the intrinsic rate constant. The increased rates are primarily due to the higher surface coverage of reactants.

For the reactions in this study, hydroisomerization of n-hexane and monomolecular cracking of n-butane and n-hexane, the rate increases upon mild steaming, i.e., the apparent rate constant increases. Furthermore, the apparent activation energy for hexane cracking is smaller or

unchanged within the uncertainty of the measurement (Fig. 2). As discussed above, similar activation energies indicate that there are not a few very strongly acidic acid sites, which account for the difference in activity. One possibility is that there is a large change in entropy. Generally, the entropy changes are small and cannot account for such large differences in activity (25). Furthermore, there is no structural model of the active site, which could account for these large differences in entropy while having no influence on the intrinsic activation energy.

There is another possibility, however. As discussed above, an increase in the enthalpy of adsorption can also lead to an increase in the apparent rate constant, Eq. [3]. The apparent activation energy would be given by Eq. [6]. For a small change to the heat of adsorption

$$\Delta H_{steam} = \Delta H_{ads} + \Delta, \qquad [7]$$

where Δ is the increase in enthalpy for the steamed zeolite. The temperature dependence of the apparent rate constant is

k_{app} (steamed zeolite)

$$= A_o * e^{-Eint/RT} * e^{-(\Delta Hads+\Delta)/RT} * e^{\Delta Sads/R} \qquad [8]$$

$$= A_o * e^{-Eint/RT} * e^{-\Delta Hads/RT} * e^{-\Delta/RT} * e^{\Delta Sads/R}. \qquad [9]$$

The experimental results reported here show that the enthalpy of adsorption at low coverages increases with steaming. However, the increase is small (<10 kJ/mol), smaller than the uncertainties in the apparent activation energy. In other words, the change in the apparent activation energy due to $e^{-\Delta/RT}$ is smaller than the error margin. Equation [9] can be simplified to

$$k_{app}(\text{steamed zeolite}) = A_1 * e^{-Eint/RT} * e^{-\Delta Hads/RT}, \qquad [10]$$

where

$$A_1 = A_o * e^{-\Delta/RT} * e^{\Delta Sads/R}. \qquad [11]$$

The decrease in apparent activation energy is not directly observed; however, the change is reflected in an altered preexponential factor according to Eq. [11]. The narrow temperature range that is generally used for the determination of an Arrhenius plot does not enable a distinction between a small change in activation energy and preexponential factor.

If one assumes that the strength of the Brønsted sites of the mildly steamed mordenite is unchanged and that the increased rate is due to an increase in the enthalpy of adsorption, then in order for the rate of n-butane cracking (at 773 K) to increase by a factor of about 3, or n-hexane isomerization (at 523 K) to increase by a factor of 7–8, the enthalpy of adsorption must increase by 3–4 kJ/mol. In other words,

$$\Delta \text{Rate (at 773 K)} = 3 = e^{-\Delta/RT}. \qquad [12]$$

While the heat of adsorption at saturation coverage of the different mordenites is not significantly different (see Fig. 7) under the reaction conditions, the surface coverage is low. This is straightforward for monomolecular alkane cracking at high temperatures. In the case of n-hexane hydroisomerization, the site-coverage with the reactive n-hexene is similarly very low, shown by the (extreme) low olefin concentration at equilibrium. Therefore, the initial enthalpies of adsorption more accurately reflect the surface coverage, which will affect the catalytic rate, Fig. 11. The difference in enthalpy of adsorption at zero surface coverage for H-MOR26 and S400 is about 5 kJ/mol and is sufficient to account for the differences in observed rates. While the difference in enthalpy between H-MOR26 and S40024 is also about 5 kJ/mol, the lower activity is due to fewer Brønsted sites. Based on the number of Brønsted sites of the two catalysts, one might expect the rate of S40024 to be higher than that of H-MOR26. For example, the increase in the heat of adsorption should lead to an increase in rate by about factor of 3. At the same time S40024 has about half the number of Brønsted sites as H-MOR26. Based on the combination of the two effects, one might expect S40024 to have slightly higher activity than H-MOR26. However, small changes in the heat of adsorption lead to significant changes in rate; thus, more precise determinations of the enthalpy of adsorption and fractional surface coverage would be required to make a more quantitative analysis. Although S40024 has lower activity for alkane cracking at 773 K than H-MOR26, S40024 is more active for hydroisomerization of n-hexane at 525 K. The relative rate for S40024 compared to H-MOR26 likely reflects the slightly higher surface coverage of n-hexane at low temperature and higher n-hexane partial pressure.

The thermodynamic data (Figs. 7–11) and the kinetic analysis suggest that the enhanced activity due to mildly steamed dealuminated zeolites can be explained by the increased enthalpy of adsorption at low surface coverage. Figure 11 shows that the initial adsorption energy increases with the increasing steam severity. Infrared spectroscopy of adsorbed pyridine indicates that the number of Lewis acid sites increases in parallel. While Lewis acid sites have previously been shown to have a higher enthalpy of adsorption of ammonia (52, 53), the tentative correlation is that Lewis acid sites also lead to an increased enthalpy of alkane adsorption. We suggested that the enhanced activity of mildly steamed mordenite is due to the increased enthalpy of alkane adsorption on Al_{EF} species (Lewis acid sites). These Lewis sites are in close contact with the Brønsted acid sites. It has been proposed that the Al_{EF} is present as widely dispersed species in the pores of a zeolite after steaming (54, 55). Moreover, Fripiat and co-workers (56) have proposed that Al_{EF} enhances activity by nonspecific synergistic effects with the Brønsted acid sites, in agreement with our proposal.

The increase in activity is due to an increase in the alkane surface coverage, rather than due to a change in the strength of the Brønsted acid strength.

CONCLUSIONS

With increasing steam partial pressure at 673 K, mild steam dealumination of H-mordenite results in the continual loss of Brønsted acid sites with a corresponding increase in the amount of Al_{EF}. As the fraction of Al_{EF} species increases, the number of Lewis acid sites increases, and the initial enthalpy of alkane adsorption increases by about 5–10 kJ/mol compared to the H-MOR without Al_{EF}. With increasing steam severity the activity initially increases and then goes through a maximum. The maximum increase in activity for n-butane monomolecular cracking and n-hexane isomerization is about 3 and 8 times, respectively, that of unsteamed mordenite.

An explanation is proposed for this (well-known) activity enhancement due to mild steaming. Under the catalytic reaction conditions, the alkane surface coverage is low. An increase in the initial enthalpy of adsorption leads to a higher surface concentration and rate. An increase of about 5 kJ/mol in the initial adsorption energy can account for the change in the observed rates. In addition, this model is consistent with temperature-dependent behavior of the apparent rate constant. Specifically, a small change in entropy of adsorption would be expected to lead to a small change in the apparent activation energy with a large increase in the preexponential factor as is observed.

REFERENCES

1. Rabo, J. A., and Gajda, G. J., *Catal. Rev. Sci. Eng.* **31**, 385 (1989).
2. Jacobs, P. A., *Catal. Rev. Sci. Eng.* **24**, 415 (1982).
3. Carson, R., Cooke, E. M., Dwyer, J., Hinchliffe, A., and O'Malley, P. J., "Zeolites as Catalysts, Sorbants and Detergent Builders," Extended Abstracts, p. 151, 1988.
4. Kassab, E., Seiti, K., and Allavena, M., *J. Phys. Chem.* **92**, 6705 (1988).
5. Barthomeuf, D., *Mat. Chem. Phys.* **17**, 49 (1987).
6. Scherzer, J., *ACS Symp. Ser.* **48**, 157 (1984).
7. Ashton, A. G., Batmanian, S., Clark, D. M., Dwyer, J., Fitch, F. R., Hinchcliffe, A., and Mochado, F. J., *in* "Studies in Surface Science and Catalysis: Catalysis by Acids and Bases" (B. Imelik *et al.*, Eds.), Vol. 20, p. 101. Elsevier, Amsterdam, 1985.
8. Lago, R. M., Haag, W. O., Mikovsky, R. J., Olson, D. H., Hellring, S. D., Schmitt, K. D., and Kerr, G. T., *in* "Proc. 7th Int. Zeolite Conf." (Y. Murakami, *et al.*, Eds.), p. 677. Kodansha, Tokyo, 1986.
9. Sendoda, Y., and Ono, Y., *Zeolites* **8**, 101 (1988).
10. Topsoe, N. Y., Joensen, F., and Derouane, E. G., *J. Catal.* **110**, 404 (1988).
11. Brunner, E., Ernst, H., Freude, D., Hunger, M., Krause, C. B., Prager, D., Reschetilowski, W., Schwieger, W., and Bergk, K. H., *Zeolites* **9**, 282 (1989).
12. Vasques, M. H., Romoa Ribeiro, F., Gnep, N. S., and Guisnet, M., *React. Kinet. Catal. Lett.* **38**, 301 (1989).
13. Zholobenko, V. L., Kustov, L. M., Kazansky, V. B., Loeffler, E., Lohse, U., Peuker, C., and Oehlmann, G., *Zeolites* **10**, 304 (1990).
14. Lukyanov, D. B., *Zoelites* **11**, 325 (1991).
15. Fritz, P. O., and Lunsford, J. H., *J. Catal.* **118**, 85 (1989).
16. Lonyi, F., and Lunsford, J. H., *J. Catal.* **136**, 566 (1992).
17. Carvajal, R., Chu, P.-J., and Lunsford, J. H., *J. Catal.* **125**, 123 (1990).
18. Haag, W. O., *in* "Zeolites and Related Materials: State of the Art 1994, Studies in Surface Science and Catalysis" (J. Weitkamp, H. G. Karge, and W. Hölderich, Eds.), Vol. 84, p. 1375. Elsevier, Amsterdam, 1994.
19. Loeffler, E., Lohse, U., Peuker, C., Oehlmann, G., Kustov, L. M., Zholobenko, V. L., and Kazansky, V. B., *Zeolites* **10**, 304 (1990).
20. Kwak, B. S., and Sachtler, W. M. H., *J. Catal.* **145**, 456 (1994).
21. Lukyanov, D. B., *Zeolites* **14**, 233 (1994).
22. Zholobenko, V. L., Kustov, L. M., Borovkov, V. Y., and Kazanskii, B. V., *Kinet. Catal.* **28**, 847 (1987).
23. Chen, F. R., and Fripiat, J. J., *J. Phys. Chem.* **97**, 5796 (1993).
24. Pieterse, J. A. Z., Seshan, K., and Lercher, J. A., *Stud. Surf. Sci. Catal.* **130C**, 2567 (2000).
25. Narbeshuber, T. F., Vinek, H., and Lercher, J. A., *J. Catal.* **157**, 388 (1995).
26. Haag, W., *Adv. Catal.* **27**, 247 (1977).
27. Williams, B. A., Babitz, S. M., Miller, J. T., Snurr, R. Q., and Kung, H. H., *Appl. Catal. A.* **177**, 161 (1999).
28. Williams, B. A., Babitz, S. M., Miller, J. T., Snurr, R. Q., Haag, W. O., and Kung, H. H., *Appl. Catal. A.* **179**, 71 (1999).
29. Denayer, J. F., Baron, G. V., Souverijns, W., Martens, J. A., and Jacobs, P. A., *Ind. Eng. Chem. Res.* **36**(8), 3242 (1997).
30. Van De Runstraat, A., Stobbelaar, P. J., Van Grondelle, J., Anderson, B. G., Van Ijzendoorn, L. J., and Van Santen, R. A., *Stud. Surf. Sci. Catal.* **105B**, 1253 (1997).
31. Tromp, M., Van Bokhoven, J. A., Garriga Oostenbrink, M. T., Bitter J. H., and Koningsberger, D. C., *J. Catal.* **190**, 209 (2000).
32. Palkhiwala, A. G., and Gorte, R. J., *Catal. Lett.* **57**, 19 (1999).
33. Glazunov, V. P., and Odinokov, S. E., *Spectrochim. Acta A* **38**, 399 (1982).
34. Miller, J. T., Hopkins, P. D., Meyers, B. L., Ray, G. J., Roginski, R. T., Zajac, G. W., and Rosenbaum, N. H., *J. Catal.* **38**, 115 (1992).
35. Kentgens, A. P. M., *Geoderma* **80**, 271 (1997).
36. Olsson, R. W., and Rollman, L. D., *Inorg. Chem.* **16**, 651 (1977).
37. Kaduk, J. A., and Faber, J., *Rigaku J.* **12**, 14 (1995).
38. Krannila, H., Haag, W. O., and Gates, B. C., *J. Catal.* **135**, 115 (1992).
39. Van Donk, S., Broersma, A., Gijzeman, O. L. Z., van Bokhoven, J. A., Bitter, J. H., and de Jong, K. P., to *J. Catal.*, submitted.
40. Van Bokhoven, J. A., and Tromp, M., in preparation.
41. Sayed, M. B., Kydd, R. A., and Cooney, R. P., *J. Catal.* **88**, 137 (1984).
42. Bordiga, S., Platero, E. E., Arean, C. O., Lamberti, C., and Zecchina, A., *J. Catal.* **137**, 179 (1992).
43. Knötzinger, H., and Ratnasamy, P., *Catal. Rev. Sci. Eng.* **17**, 31 (1978).
44. Zholobenko, V. L., Makarova, M. A., and Dwyer, J., *J. Phys. Chem.* **97**, 5962 (1993).
45. Gates, B. C., Katzer, J. R., and Schuit, G. C., "Chemistry of Catalytic Processes." McGraw–Hill, New York, 1979.

46. Haag, W. O., and Dessau, R. M., *in* "Proceedings, 8th International Congress on Catalysis," Berlin, 1984, Vol. 2. p. 305.
47. Weisz, P. B., *Adv. Catal.* **13**, 137 (1962).
48. Williams, B. A., Babitz, S. M., Ji, W., Miller, J. T., Snurr, R. Q., and Kung, H. K., submitted for publication.
49. Hong, X., Gruver, V., and Fripiat, J. J., *J. Catal.* **150**, 421 (1994).
50. Babitz, S. M., Kuehne M. A., Kung H. H., and Miller, J. T., *Ind. Eng. Chem. Res.* **36**, 3027 (1997).
51. Wei, J., *Chem. Eng. Sci.* **51**, 2995 (1996).
52. Kuehne, M. A., Kung, H. H., and Miller, J. T., *J. Catal.* **171**, 293 (1997).
53. Kuehne, M. A., Babitz, S. M., Kung, H. H., and Miller, J. T., *Appl. Catal. A: Gen.* **166**, 293 (1998).
54. Beyerlein, R. A., Choi-Feng, C., Hall, J. B., Huggins, B. J., and Ray, G. J., *Top. Catal.* **4**, 27 (1997).
55. Van Bokhoven, J. A., Roest, A. L., Nachtegaal, G. H., Kentgens, A. P. M., and Koningsberger, D. C., *J. Phys. Chem. B.* **104**, 6743 (2000).
56. Hong, Y., Gruver, V., and Fripiat, J. J., *J. Catal.* **150**, 421 (1994).